ELSEVIER

Chemical Engineering Journal 141 (2008) 58–66

Chemical Engineering Journal

www.elsevier.com/locate/cej

On line analysis of structure of dispersions in an oscillatory baffled reactor using electrical impedance tomography

G. Vilar [a,*], R.A. Williams [a], M. Wang [a], R.J. Tweedie [b]

[a] *Institute of Particle Science & Engineering, Houldsworth Building, University of Leeds, Clarendon Road, Leeds LS2 9JT, United Kingdom*

[b] *Malvern Instruments Ltd., Enigma Business Park, Grovewood Road, Malvern WR14 1XZ, United Kingdom*

Received 6 March 2007; received in revised form 17 July 2007; accepted 17 October 2007

Abstract

A novel methodology of on line measurement in an oscillatory baffled reactor (OBR) is presented. We show how the use of an electrical impedance tomography (EIT) sensor can map the spatial concentration of the dispersed phase in the emulsion and also obtain velocity profile information. Data are presented based on experimental work to enable production of water-in-oil/oil-in-water emulsions using the results of the on line measurement with the EIT. Process performance is quantified using dimensionless parameters of the OBR and the data obtained from cross-correlation of tomographic signals. The velocity results derived from the EIT data show good agreement with the well known flow pattern of the OBR described in previous works. The application of Maxwell relations enables the quantification of the local oil volume distribution in the emulsion process. Research demonstrates the principle how such methods can be used to monitor a chemical process in the OBR using electrical impedance tomography.

Keywords: Online analysis; Tomography sensor; Oscillatory baffled reactor

1. Introduction

The development of new personal products and other ‘fast moving’ consumer goods is an important challenge for the continued competitiveness in innovation and manufacturing. This research explores a new paradigm for formulation multi-component emulsions. It enables new products to be made consistently but in radically simplified equipment and on a semi-continuous basis. Target application examples include precision manufacture of emulsions, microcapsules and solid particulates in an oscillatory baffled reactor (OBR). This paper explores product formulation in a pipeline containing baffles by combining, for the first time, novel advanced techniques of on-line imaging instrumentation based on electrical impedance tomography (EIT) and the new chemical reactor technology.

Many chemical manufacturing processes that were implemented possible in batch previously can be performed in the OBR operating as a continuous reactor. This is the principal advantage of this type of reactor but may also enable added versatility. The transition from batch to semi-continuous operation using this alternative technology presents an industrial challenge but is of widespread interest to a number of manufacturing sectors [1].

1.1. Oscillatory baffled technology

An OBR consists of a continuous reactor built of equally spaced orifice plate baffles. The main characteristic of these reactors is that the process fluid has an oscillatory movement that is superimposed upon all the fluid in the reactor (Fig. 1). This means that the direction of the fluid in the reaction is not following a linear movement: The addition of a sinusoidal imposed movement enables the radial mixing unlike the traditional plug-flow reactors.

The orifice plate baffles are one of the important parts of the reactor due to their influence in the formation of vortex cycles in the direction of the process fluid. The combination of baffles and the oscillatory movement creates a flow pattern that is leading to highly efficient heat and mass transfer while maintaining plug flow. Fig. 2 describes the flow pattern of an OBR and a

* Corresponding author.
E-mail address: pre4gvu@leeds.ac.uk (G. Vilar).

1385-8947/$ – see front matter © 2007 Elsevier B.V. All rights reserved.
doi:10.1016/j.cej.2007.10.018

Nomenclature

a, b	constants
C_V	volume fraction
d_{32}	droplet size (μm)
d_{32s}	droplet size average value after transitional time (μm)
D	diameter of the tube (m)
f	oscillation frequency (Hz)
(n,m)	coordinates of the pixel
P	shift number in time sequence of frames
P1	first plane of electrodes
P2	second plane of electrodes
Re_n	net flow Reynolds number
Re_o	oscillatory Reynolds number
Str	Strouhal number
t	elapsed time (s)
T	number of images for which the cross-correlation is calculated
$V_{P1}[k]$	numerical values associated with pixel n from image k obtained from plane P1
V_{P2}	$[k+p]$ numerical values associated with pixel n from image $k+p$ obtained from plane P2
x_0	oscillation amplitude (m)

Greek letters

μ	dynamic viscosity of the flow (kg/m s)
ρ	density of the flow (kg/m^3)
σ_C	conductivity of the continuous phase (mS/cm)
σ_D	conductivity of the dispersed phase (mS/cm)
σ_M	conductivity of the mixture (mS/cm)
Ψ	velocity ratio

comparison with a previous work using digital particle image velocimetry (DPIV) [2].

The oscillatory flow improves the mixing of the materials due to the combination of the baffles that cause to reverse periodically the flow in the channel. In this way, the vortices are produced on the downstream side of each baffle following each flow reversal interact with each other in a complex way [3]. The radial velocity is high due to the mixing within each inter-baffle [4]; this mechanism is taking advantage of the vortices that are produced in the inter-baffle cavities to improve radial mixing. Unlike conventional plug-flow reactors, where a minimum Reynolds number must be maintained, radial mixing is independent of the net flow. This is one of the main advantages of the OBR, because this allows long residence times (of order of hours) to be achieved in a reactor of greatly reduced length-to-diameter ratio.

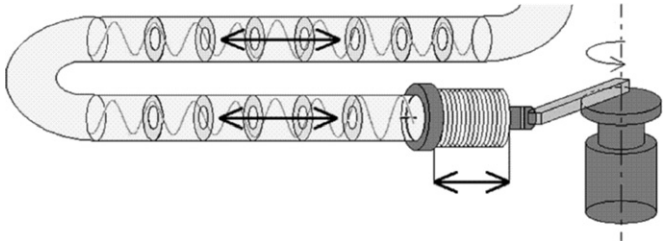

Fig. 1. Superimposed oscillatory movement in the oscillatory baffled reactor.

Since, the OBR reactor takes advantage of the radial mixing and vortex formation, consequently, the volume of the reactor is used more efficiently because the process of mixing is improved due to the increase of the contact in the same amount of volume. This is achieved while maintaining plug-flow residence time distribution (RTD) characteristics, effective mixing, and high heat and mass transfer rates. These features allow a better performance of the reactor. In design terms of the length of the reactor, the same conversion of the product in a traditional plug-flow reactor can be achieved whilst maintaining the same diameter. The uniformity of performance all along the reactor depends on the specific process since it is evident that is the fluid viscosity or other physical properties change downstream the conversion characteristics will also be mediated. This is not considered in the present work.

The characteristics of the flow in an OBR have been discussed on detail by Gough and Ni [5]. Their main research is based in the modification of the flow pattern by the oscillatory vortices due to the superimposed sinusoidal pulse. The fluid mechanical conditions in OBR are governed by four dimensionless groups given below:

1. The Oscillatory Reynolds number Re_o describes the intensity of mixing applied to the column. In steady flow, the Re_o is an indicator of the relative importance of the inertial and viscous forces. Re_o is similar to the conventional number Re_n for steady flows, but the velocity term used is the maximum velocity of a sinusoidal oscillation. This allows a wide range of mixing conditions to be achieved, from "soft" mixing, where Re_o is in the range of 50–500, to the most intense, corresponding to mixed flow (a single continuous stirred tank reactor, CSTR), where Re_o is over 5000.

$$Re_o = \frac{2\pi x_0 f \rho D}{\mu} \quad (1)$$

where x_0 is the oscillation amplitude, f is the oscillation frequency, ρ is the density of the flow, D is the diameter of the tube and μ is the viscosity of the flow.

2. The net flow Reynolds number Re_n describes the imposed type of flow in the reactor. If Re_n is higher than 2100 then it is considered that the liquid of the reactor is in a turbulent regime. It depends on the velocity of the flow v.

$$Re_n = \frac{\rho D v}{\mu} \quad (2)$$

3. The velocity ratio ψ is an indicator of the oscillation produced in comparison to velocity of the net flow. It is necessary for the oscillatory flow to be dominant for the full effect of the vortex cycle to be realized, the flow should be fully reversing. For this condition to be satisfied, ψ must be between 4 and 10.

$$\Psi = \frac{Re_o}{Re_n} \quad (3)$$

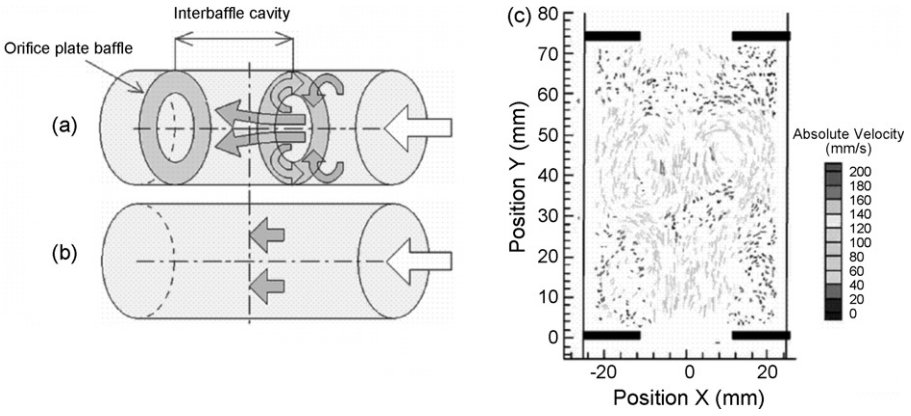

Fig. 2. Comparison of mixing between plug flow (b) and OBR (a) and DPIV (c) (adapted from Ni et al. [2]).

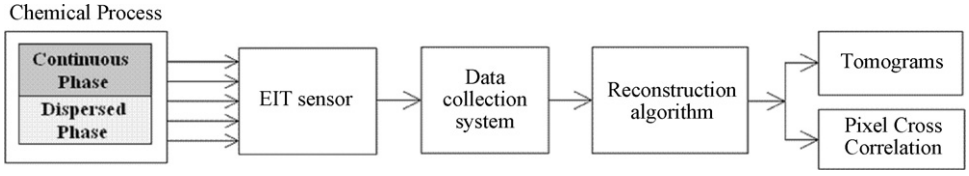

Fig. 3. Block diagram of the data processes using electrical impedance tomography.

The principle of the operation of the OBR is based on superimposing an oscillatory movement upon all the fluid that is in a laminar flow regime inside the pipe ($Re_n < 2100$). This means that this oscillatory movement should be enough powerful to make the fluid loop and reverse (oscillatory Reynolds number Re_o must be at least 4 times higher than the net flow Reynolds number Re_n). When the net flow is in turbulent flow, net flow Reynolds number Re_n can have a huge and variable value that means it is necessary to define an additional parameter called the Strouhal number.

4. The Strouhal number represents the amplitude ratio of oscillation; it is the ratio of column diameter to stroke length, measuring the effective eddy propagation. The larger the Strouhal number, the smaller the amplitude of oscillation.

$$Str = \frac{D}{4\pi x_0} \tag{4}$$

where x_0 is the oscillatory amplitude, and D is the diameter of the pipe.

1.2. Electrical impedance tomography

Electrical impedance tomography (EIT) is an emerging technique that can be used for mapping the concentration, and to measure velocity distributions in two-phase flows, where electrical conductivity or permeability differences exist between the two-phase fluids [6]. The measurement of the different impedance of the two-phase fluids in a chemical process, the analysis of the data and the conversion to different variables (velocity, concentration, etc.) are the main steps in the control of a process by the EIT technique.

The application of the EIT technique is limited by a number of factors, which are the transient time of ac coupling interface, the speed of signal demodulation, the extensive computation from on line image reconstruction and velocity implementation, and the speed of data transmission [7]. The objective of the EIT sensor is the detection of differences of concentration that sensed through detecting changes in local electrical impedance. The measurement of the impedance in the dispersed phase in a multiphase flow is sensed by the EIT sensor which consists of point electrodes mounted on the inner periphery on the pipe wall in a circular array (see Section 2). Its data acquisition system (DAS) injects the electrical current flow between one pair of adjoining electrodes and then the different potentials between all outstanding pairs of adjacent electrodes are measured. In the system used in this experiment the minimum difference in the conductivity detectable is 10^{-3} mS/cm.

The DAS transforms the electrical signal into raw data (Fig. 3), these data are processed by a reconstruction algorithm. The result is the reconstruction of the image that shows an estimate of the mapping of the distribution of concentration of the two-phase flow in the chemical process [7]. The DAS used in the experimental work is the ITOMS[1] P2000 System (Industrial Tomography Systems, Manchester, UK) and the reconstruction algorithm used is based on linear back projection algorithm [8].

The measurement of the impedance difference of the two-phase fluid in the OBR enables the mapping of the concentration of the fluid. The concentration calculation is based on the application of Maxwell relationship (Maxwell [9]; Lucas et al. [10]; George et al. [11]):

$$C_V = \frac{2\sigma_E + \sigma_D - 2\sigma_M - ((\sigma_M\sigma_D)/\sigma_C)}{\sigma_M - (\sigma_D/\sigma_C) + 2(\sigma_C - \sigma_D)} \tag{5}$$

[1] ITOMS Industrial Tomography Systems. 47 Newton Street, Manchester, M1 1FT, United Kingdom. Tel: +44 161 237 5779; fax: +44 161 237 5669.

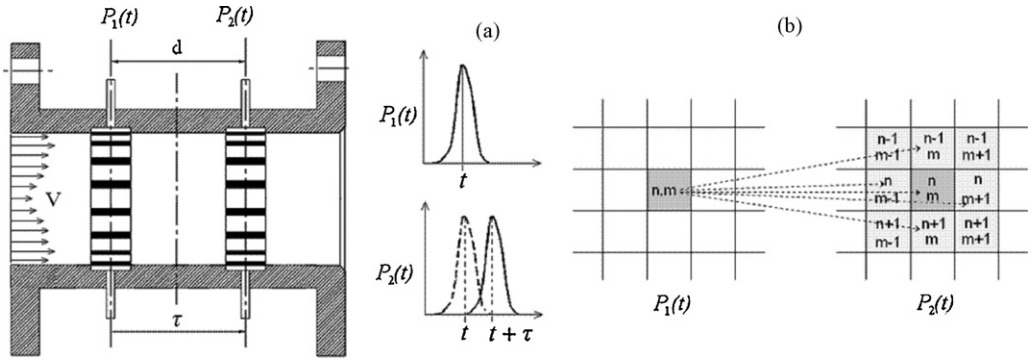

Fig. 4. Application of pixel-based cross-correlation method (adapted from Mosorov et al. [15]).

where C_V is the volume fraction, σ_C is the conductivity of the continuous phase, σ_D is the conductivity of the dispersed phase and σ_M is the conductivity of the mixture. If the dispersed phase is assumed to be non-conductive, then Eq. (5) can be simplified to:

$$C_V = \frac{2\sigma_C - 2\sigma_M}{\sigma_M + 2\sigma_C} \tag{6}$$

According to Maxwell, the validity of Eq. (5) is limited to small volume fraction, however, various researchers found that Eq. (5) produced good agreement with experimental data over a wide range of void fractions (Neale and Nader [12], Wu et al. [13]).

1.3. Application of pixel-based cross-correlation method

Cross-correlation methods have been recently discussed to obtain velocity profiles using EIT as a measurement technique. The application of cross-correlation software (CCS[2]) is based on the comparison of the conductivity data (tomograms) obtained from one plane of electrodes (P1) with the data obtained from another plane of electrodes (P2) where the distance between planes of electrodes is known. Considerable research has been conducted in cross-correlation for developing a suitable method of measurement of velocity distributions in industrial applications [14].

The concept of the best correlated pixel method by Mosorov et al. is used to calculate flow velocities for a number of applications using EIT as a measurement technique [15]. The cross-correlation function is defined by the following equation:

$$R_{P1,P2}(\tau) = \lim_{T\to\infty} \frac{1}{T} \int_0^T P1(t)P2(t+\tau)dt \tag{7}$$

The functions P1 and P2 are the detected signals from the planes 1 and 2 (Fig. 4a), respectively, τ is a time delay and T is a time period for which the cross-correlation is calculated.

In the classical cross-correlation methods, only corresponding pixels are correlated, but this hypothesis can be improved. The method proposed by Mosorov et al. [15] is based on the assumption that a signal from one pixel on the first plane (P1) is sometimes better correlated with a signal from a non-corresponding pixel on the second plane (P2) than with a corresponding pixel (Fig. 4b). In this paper the method is discussed in detail, and several examples where a pixel from P1 is best correlated with a non-corresponding pixel on plane P2 are shown. In particular, in one experiment the chosen pixel was best correlated with a non-corresponding pixel in about 17% of the cases.

In this method the pixels from the second plane are chosen from the corresponding pixel and its neighbours, which gives better correlation. This means that this method is more independent of the flow pattern; therefore, this concept is very important due to the complex flow pattern of the OBR. The best correlated pair is taken from the correlation calculations. The correlation function between a pixel from plane 1 with several pixels from the plane 2 can be obtained by:

$$R_{P1[n,m]P2[n-i,m-j]}[p] = \sum_{K=0}^{T-1} V_{P1[n,m]}[k]V_{P2[n-i,m-j]}[k+p], \quad (i,j) \in B \tag{8}$$

In the above equation (n,m) are the coordinates of the pixel; p is the shift number in time sequence of frames, T is the number of images for which the cross-correlation is calculated; $V_{P1}[k]$, $V_{P2}[k+p]$ are the numerical values associated with pixel n from image k obtained from plane P1 and from image $k+p$ obtained from plane P2, respectively. V_{P1}, V_{P2} are the value of the pixel (n,m) on planes 1 and 2; B is the neighbourhood of pixel (n,m) on plane 2 (Fig. 4b).

2. Experimental arrangements

The OBR consist of a continuous chemical reactor where equally spaced orifice plate baffles are firmly positioned inside the main pipe. The oscillatory movement is imposed by a piston drive where the oscillation frequency and amplitude are constant. The water flow (continuous phase) is supplied by an external pump. A mineral oil (dispersed phase) is added from an insertion point of the pipe to generate the emulsion (Fig. 5) and the EIT sensor is installed in the end of the pipe (Fig. 6). The EIT sensor has 2 planes of 16 electrodes and the distance between the planes is 30 mm. This separation distance enables the application

[2] CCS Cross Correlation Software version 2.0. Institute of Mechanics, Chinese Academy of Sciences and Institute of Particle Science and Engineering, University of Leeds. Copyright 2004.

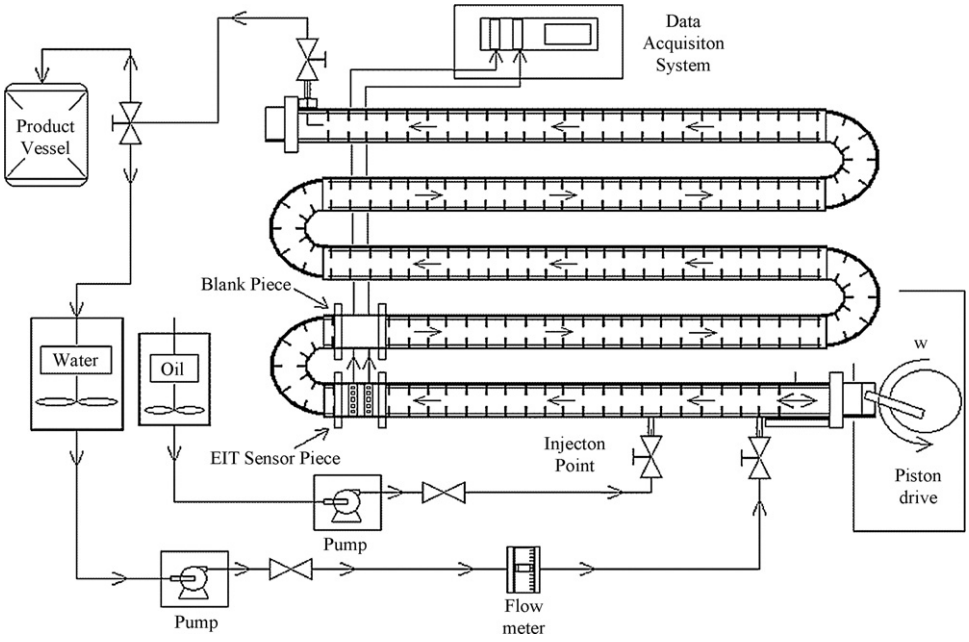

Fig. 5. Experimental set-up of the OBR.

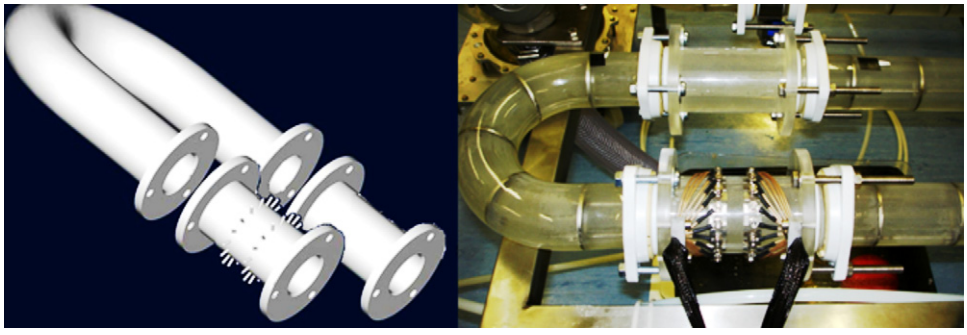

Fig. 6. EIT sensor with 2 planes of 16 electrodes in the OBR.

of the proposed pixel-based cross-correlation method between the two planes of electrodes accurately. The conductivities of the continuous phase and dispersed phase were measured individually with the EIT sensor; the results of the characteristics of the emulsion are reported in Table 1.

3. Results

3.1. Objective of experimental work

The objective of the experimental work is to determine the characteristics of the oil-in-water emulsion and to monitor the process in the OBR through an EIT sensor. The experimental measurement of the variables was carried though the measurement of the oil droplet size through digital image analysis (Fig. 7). A high-speed digital camera was used to capture all images of droplets through the experiment. The camera operates with a maximum frequency of up to 30 images per second with a typical pixel resolution of 640 × 480 and a field of view from 140 μm to 16 mm. Images were taken in intervals of 1 min at different positions along the all the tube in order to measure the evolution of droplet size in the entire OBR. The times at which droplets arrived at different locations along the reactor were noted. The digital camera provided a sequence of high definition images of droplets. The selection of the images and the processing with the digital image analysis software ImageJ[3] enabled the characteristic droplet size and droplet size distribution evolution to be obtained within the OBR at different times (Fig. 8).

Table 1
Characteristics of the emulsion

Measured properties (at 21 °C)	Conductivity (mS/cm)	Density (kg/m^3)	Kinematic viscosity (m^2/s)
Water	1.310	997	0.8935×10^{-6}
White mineral oil (CAS-No.8042-47-5)	0.078	850	15.5×10^{-6}

[3] ImageJ is being developed at the National Institutes of Health by an employee of the Federal Government in the course of his official duties. Pursuant to Title 17, Section 105 of the United States Code, this software is not subject to copyright protection and is in the public domain (http://rsb.info.nih.gov/ij/).

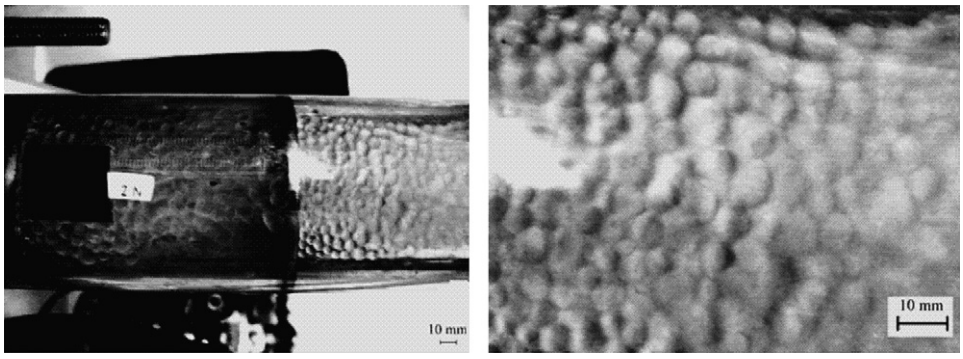

Fig. 7. Oil droplets in the OBR.

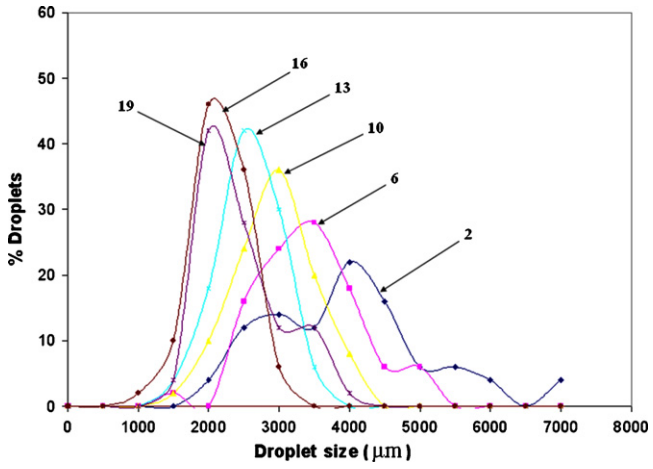

Fig. 8. Measurements of droplet size distributions with time (min).

The analysis of the images was carried using ImageJ. This software is being developed at the National Institute of Health by the US Federal Government.

3.2. Analysis of dispersion structure

The emulsion process was continuously monitored through the EIT sensor in the OBR. The parameters for control of the OBR were constant through the experiment (Table 2).

The oscillatory Reynolds number Re_o was higher than 5000, which means a high intensity of oscillation. The value of the velocity ratio Ψ is determining that the oscillation (Re_o) is clearly superimposed upon the net flow (Re_n) (Table 3).

The decreasing trend of the droplet size with time was found to be an exponential correlation by Hong and Lee [16] and Zerfa and Brooks [17] as:

$$\frac{d_{32}}{d_{32s}} = 1 + a\exp(-bft) \rightarrow \ln\left(\frac{d_{32} - d_{32s}}{d_{32s}}\right) = \ln(a) - bft \quad (9)$$

where d_{32} is the droplet size, d_{32s} is the droplet size average value after transitional time, f is the oscillatory frequency, t is the elapsed time, and a, b are constants. The fitting of the dimensionless term of $\ln(d_{32} - d_{32s}/d_{32s})$ vs. the dimensionless time term of ft, gives a straight line ($R^2 = 0.9699$) where $a = 1.981$ and $b = 0.00084$ (Fig. 9). These constants are of a similar order of magnitude as earlier studies in stirred tank reactors ($a = 1.0$ and $b = 0.00017$ in STRs) which means that the transitional droplet behaviours in OBR are compatible to those in STRs [18].

The results of the decreasing trend of the droplet size with processing time shows good agreement with previous studies in water-in-oil emulsions carried out in an OBR [19].

Table 2
Parameters of control of the OBR

Properties	Experimental values
Oil flow rate (m^3/s)	1.667×10^{-6}
Oscillation frequency (Hz)	2
Oscillation amplitude (m)	0.012
Diameter of the pipe (m)	0.05
Diameter of the orifice (m)	0.023

Table 3
Non-dimensional parameters in the OBR

Properties			
Re_o	Re_n	Ψ	Str
8439	2090	4.038	0.332

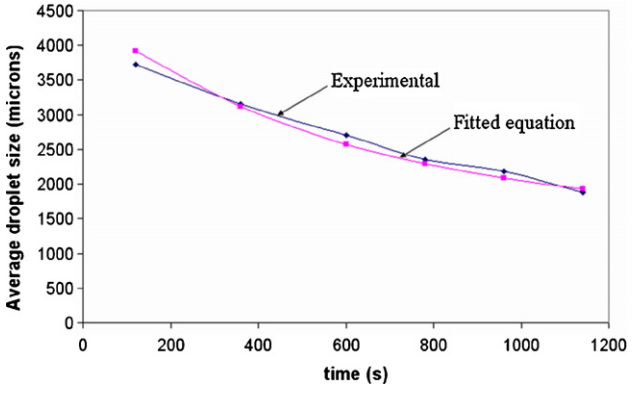

Fig. 9. Decreasing droplet size with time.

3.3. Monitoring of dispersion structure

The measurement of the impedance of the mineral oil (dispersed phase) in the emulsion with the EIT sensor and the application of the reconstruction algorithm (Fig. 3) enables to obtain the conductivity of the fluid in each one of the planes of electrodes (tomograms). Two different experiments were carried out using a water net flow of 6.667×10^{-5} and 7×10^{-5} m^3/s for experiments 1 and 2, respectively. The small difference of net flow rates is due to a difficulty of setting and maintaining the exact flow rate due to the high oscillation, however the EIT measurement is not affected considerably. The frequency and amplitude were set to the same conditions described by Table 2. A total number of 600 tomograms were acquired for each experiment. The application of Eq. (6) in the conductivity measurements (mS/cm) leads to the mapping of the oil volume fraction (C_V) in the emulsion for both experiments (Fig. 10).

The mapping of the local oil volume fraction shows the characteristic flow pattern in the OBR (Fig. 2). The oil is dispersed as droplets into the water, as shown in Fig. 7. The density of the oil (850 kg/m^3) is much lower than the water (997 kg/m^3), which means that even though the flow is in a high mixing regime, part of oil is moving to the top radial edge of the pipe. Hence, the minimum conductivity measured (around 0.1 mS/cm) which means the maximum oil volume fraction (C_V around 0.88) in the tomograms (Fig. 10a). The oil fraction is mixing together with the water, as it can seen in Fig. 10c, where the values of conductivity are around 0.7 mS/cm, which means that the oil volume fraction (C_V) in that zone is around 0.4. This means that the oil flow moves to the central bore of the pipe creating vortex cycles, following OBR flow pattern. This also can be seen in Fig. 10b, the conductivity of the mixture is maximum (around 1.2 mS/cm) which means that the oil volume fraction in the centre of the pipe reach its minimum (0.055), due to the vortex formation, the oil flow moves to the bore of the pipe showing the radial mixing (Fig. 10c). The information on the conductivity measurements and the calculation of the oil volume fraction allow describing spatially the mixing process in the OBR (Fig. 11).

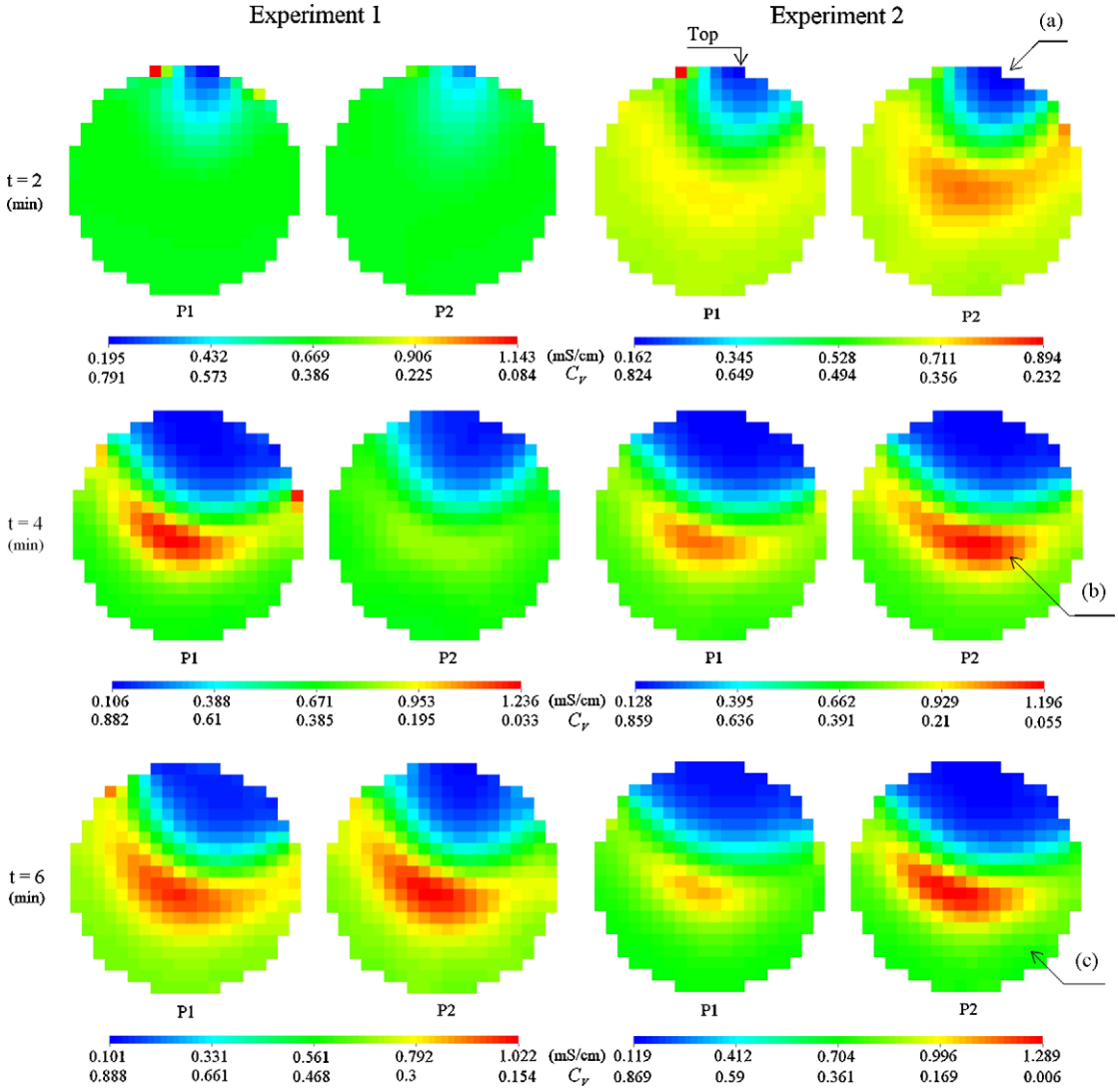

Fig. 10. Conductivity measurements and local oil volume fraction distributions.

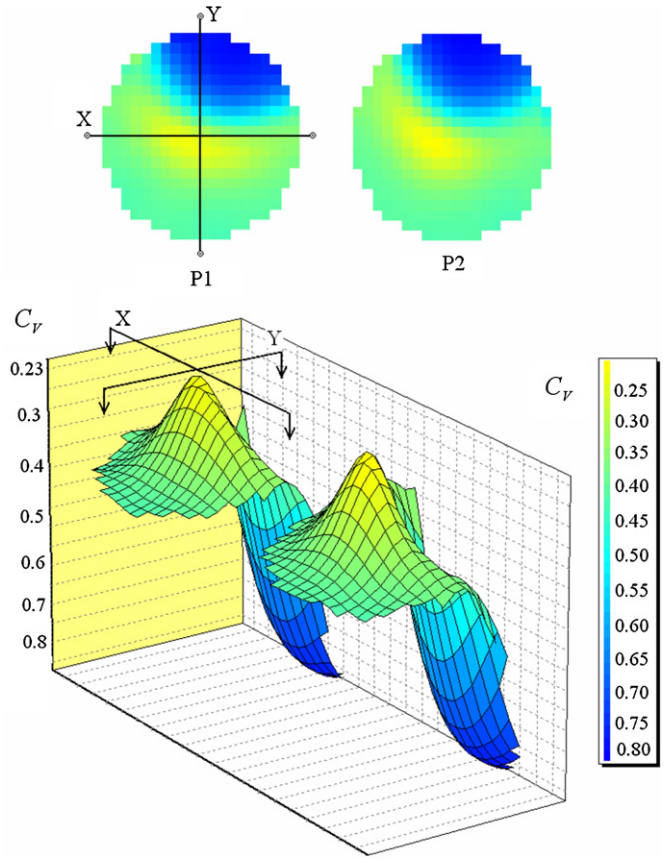

Fig. 11. Tomograms and reconstruction of the oil volume distribution (Experiment 1, $t = 6$ min).

The application of cross-correlation method (Eq. (8)) to the data obtained from the tomograms enables the velocity profiles in the *X*- and *Y*-planes of the dispersed phase in the OBR to be estimated. Fig. 12 shows a representation of the velocity of the dispersed phase in the planes *X* and *Y* with the relation radius/diameter (*r*/*D*) of the pipe (Figs. 12 and 13). The direction of the *X*- and *Y*-planes is described in Fig. 11.

The local velocity distribution in the plane *X* (Fig. 12) shows a higher velocity of the dispersed phase near the bore of the pipe (0.006 m/s in $r/D = 0.25$). This is due to the vortices created by the oscillatory superimposed movement (Fig. 2a). The local velocity distribution in the plane *Y* (Fig. 13) shows a higher velocity of the dispersed phase near the top of the pipe (0.025 m/s in $r/D = 0.375$). This is due to the accumulation of oil droplets

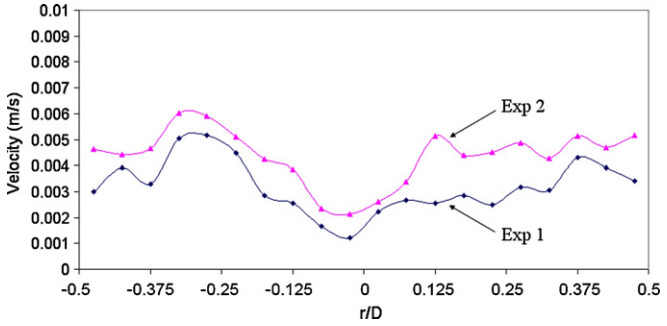

Fig. 12. Local velocity distribution of the dispersed phase in the plane *X*.

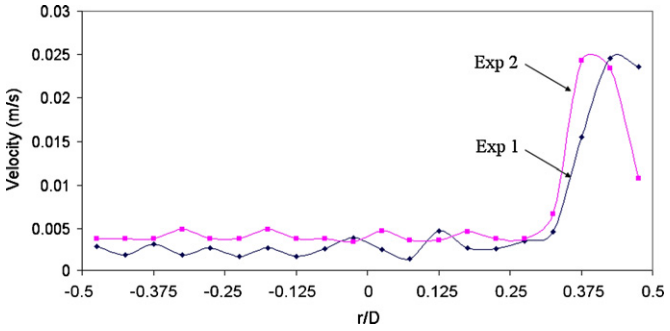

Fig. 13. Local velocity distribution of the dispersed phase in the plane *Y*.

towards the top radial edge of the pipe (Fig. 10a) caused the lower density of the oil respect the water (Table 1).

The results show the comparison between both experiments. In this study good agreement between the results obtained from the two experiments has been achieved. The comparison of the calculated velocity profiles (Figs. 12 and 13) and the reconstruction of the oil volume distribution (Fig. 11) with the described OBR flow pattern (Fig. 2) indicate that the obtained results are consistent. The differences between experiments may be caused by:

- While there is, helpfully, a strong contrast in electrical impedance provided by the oil and volume fraction used enabling opportunities for conductivity mapping (Fig. 10), there is potential for the large droplets produced to coalesce and/or to gather in the vicinity of electrodes in the upper section of the pipe (Fig. 10a). This can have the consequence of some electrodes losing electrical contact with water, so some measurement from these electrodes could be erroneous [14]. The comparison of the values of the pixels located on the top of the pipe with the mean value calculated gives a deviation of less than 6%.
- The overall velocity of the flow is slow (Figs. 12 and 13) compared to previous studies using cross-correlation method (10 m/s) [15], but there is a significant variation of flow speed due to the superimposed sinusoidal flow (Table 2). This means that the cross-correlation method based on EIT may be not able to detect completely the smaller changes in conductivity measurements (superimposed movement of oil in Fig. 10c, zone of high mixing) and velocity profiles due to the high acceleration of the fluid. However, the comparison of the values of oil volume fraction obtained for different times (Fig. 10) indicates that the dispersed phase follows a clear steady flow pattern. The variation found between the values in different zones (maximum oil volume fraction C_V around 0.88 (Fig. 10a) and minimum oil volume fraction C_V around 0.055 (Fig. 10b) and a mean value of oil volume fraction calculated for each one of these zones is less than 8%, which means good accuracy of the EIT measurements. A faster acquisition of tomograms would help to improve the cross-correlation between the two planes of electrodes. The OBR flow pattern is complex and further study in correlation methods is in progress.

4. Conclusions

A novel methodology of on line measurement in an OBR is presented. The analysis of the structure dispersion enables the description and prediction of the characteristics of the oil-in-water emulsion and the energy consumption of the process. The experimental work demonstrates the feasibility of production of water-in-oil/oil-in-water emulsions and, for the first time, monitoring a chemical process in the OBR through use of an EIT sensor. The results show the droplet size as a function of the frequency and amplitude.

Tomographic measurements reveal the concentration of the dispersed phase in the emulsion. The measurement of the impedance of the dispersed phase shows a clear mapping of the emulsion process in the OBR in time. The results shown in Fig. 10 and the reconstruction of oil volume distribution in Fig. 11 show good agreement with the well known flow pattern of the OBR described in previous works (Fig. 2c). The application of Maxwell relation enables to quantify accurately the local oil volume distribution for each measurement in the OBR.

The application of cross-correlation method to the data obtained from the tomograms demonstrates the capability of the system to obtain the velocity profiles of the dispersed phase in the flow. Further study in improvement of application of the cross-correlation method is in progress.

Acknowledgement

The authors are grateful to studentship funding from the Virtual Centre for Industrial Process Tomography, University of Leeds and for collaboration with Malvern Instruments in this work.

References

[1] K. Plumb, Continuous processing in the pharmaceutical industry: changing the mind set, Chem. Eng. Res. Des. 83(A6) (2005) 730–738.
[2] X. Ni, H. Jian, A.W. Fitch, Computational fluid dynamic modelling of flow patterns in an oscillatory baffled column, Chem. Eng. Sci. 57 (2002) 2849–2862.
[3] C.R. Brunold, J.C.B. Hunns, M.R. Mackley, J.W. Thompson, Experimental observations on flow patterns and energy losses for oscillatory flow in ducts containing sharp edge, Chem. Eng. Sci. 44 (1998) 1227–1244.
[4] T. Howes, M.R. Mackley, E.P.L. Roberts, The simulation of chaotic mixing and dispersion of periodic flows in baffled channels, Chem. Eng. Sci. 48 (1991) 799–803.
[5] P. Gough, X. Ni, On the discussion of the dimensionless groups governing oscillatory flow in a baffled tube, Chem. Eng. Sci. 52 (1997) 3209–3212.
[6] M. Wang, Impedance mapping of particulate multiphase flows, Flow Meas. Instrum. 16 (2005) 183–189.
[7] M. Wang, F.J. Dickin, Electrical resistance tomography for process applications, Meas. Sci. Technol. 7 (1996) 247–260.
[8] M. Wang, Inverse solutions for electrical impedance tomography based on conjugate gradients methods, Meas. Sci. Technol. 13 (2002) 101–117.
[9] J.C. Maxwell, A Treatise on Electricity and Magnetism, Clarendon Press, Oxford, UK, 1881.
[10] G.P. Lucas, J. Cory, R. Waterfall, W.W. Loh, F.J. Dickin, Measurement of the solids volume fraction and velocity distributions in solid-liquid flows using dual-plane electrical resistance tomography, J. Flow Meas. Instrum. 10 (1999) 249–258.
[11] D.L. George, J.R. Torczynski, K.A. Shollenbeger, T.J. O'henand, S.L. Ceceio, Validation of electrical-impedance tomography for measurements of material distribution in two-phase flows, Int. J. Multiphase Flow 26 (2000) 549–581.
[12] G.H. Neale, W.K. Nader, Prediction of transport process within porous media: diffusion flow processes within an homogeneous swarm of spherical particles, AICHE J. 19 (1973) 112–119.
[13] Y. Wu, L. Hua, M. Wang, R.A. Williams, Characterization of air-water two-phase characterization of air-water two-phase vertical flow by using electrical resistance vertical flow by using electrical resistance imaging, Can. J. Chem. Eng. 83 (2005) 37–41.
[14] L. Hua, M. Wang, Y. Wu, Y. Ma, R.A. Williams, Measurement of oil volume fraction and velocity distributions in vertical oil-in-water flows using ERT and a local probe, J. Zheiiang Univ. SCI 6A (12) (2005) 1412–1415.
[15] V. Mosorov, L. Sankowski, L. Mazurkiewicz, T. Dyakowski, The 'best-correlated pixels' method for solid mass flow measurements using electrical capacitance tomography, Meas. Sci. Technol. 13 (2002) 1810–1814.
[16] P.O. Hong, J.M. Lee, Unsteady-state liquid-liquid dispersions in agitated vessels, Ind. Eng. Chem. Process Des. Dev. 22 (1983) (1983) 130–135.
[17] M. Zerfa, B.W. Brooks, Vinyl-chloride dispersion with relation to suspension polymerization, Chem. Eng. Sci. 51 (1996) 3591–3611.
[18] X. Ni, Y. Zhangt, I. Mustafa, An investigation of droplet size and size distribution in methylmethacrylate suspensions in a batch oscillatory baffled reactor, Chem. Eng. Sci. 53 (1998) 2903–2919.
[19] D. Mignard, L.P. Amin, X. Ni, Determination of breakage rates of oil droplets in a continuous oscillatory baffled tube, Chem. Eng. Sci. 61 (2006) 6902–6917.